

Investigation on trapping capability of circular swallowtail beams

Huanpeng Liang,¹ Xiaofang Lu,¹ Kaijian Chen,¹ Haixia Wu,¹ Nana Liu,¹ Liu Tan,¹ Shaozhou Jiang,¹ and Yi Liang^{1,*}

¹*Guangxi Key Lab for Relativistic Astrophysics, Center on Nanoenergy Research, Guangxi Colleges and Universities Key Laboratory of Blue Energy and Systems Integration, School of Physical Science and Technology, Guangxi University, Nanning, Guangxi 530004, China*
(Dated: December 5, 2023)

Circular swallowtail beams (CSBs) with their remarkable autofocusing capability have garnered significant interests due to their potential applications in optical trapping. This study delves into a comprehensive investigation of the trapping force properties of CSBs. Through a combination of experimental observations and theoretical analysis, we systematically explore the quantitative manipulation of trapping forces by adjusting specific parameters. This detailed investigation provides insights into the trapping force performance and stability of CSBs. Furthermore, the experimental validation of particle trapping using CSBs underscores their effectiveness, emphasizing their significant potential for optical manipulation and trapping applications.

I. INTRODUCTION

Various accelerating beams that propagate along curved trajectories have attracted a lot of attention due to a huge potential for many applications including optical tweezers[1–3], biomedical science[4, 5], astrophysics[6]and so on. The most famous accelerating beams, named Airy beams[7–12], are experimentally generated in 2007. Airy beams can be described as a result of the fold catastrophe in catastrophe theory. There are seven fundamental catastrophes including fold[7], cusp[13], swallowtail[14], butterfly[14], elliptical umbilic[15], hyperbolic umbilic[16], and parabolic umbilic[17]. Most beams related to these catastrophes can present a curve propagation trajectory, i.e., and therefore they can be employed to generate an accelerating beam. For example, a family of accelerating beams, called Pearcey beams[13, 18], comes from the cusp catastrophe. Recently, originating from swallowtail catastrophe, a new kind of high-order accelerating beams named Swallowtail beams are generated[19]. Swallowtail beams exhibit a unique feature: by tuning control parameters, Swallowtail beams not only can evolve into higher-order butterfly catastrophes during propagation, but also can decay to lower-order cusp catastrophe such as Pearcey beams.

As we know, the autofocusing properties of autofocusing beams[20–24]generated from accelerating beams is determined by the acceleration of the beams. The autofocusing propagation of circular Airy beams (CABs) can be modulated by tuning the parameters related to acceleration of Airy beams including the scale factor and initial position of main lobe[25]. Along this line, one can infer that autofocusing beams based on Swallowtail beams such as Circular swallowtail beams (CSBs) also show a similar autofocusing property, as demonstrated in Refs.[14, 26–31]. Due to this autofocusing property, CSBs exhibits a stronger intensity contrast at the auto-

focusing position, which means that it has great potential for optical manipulation or trapping. However, as far as we know, trapping force and the trapping stability of CSBs lacks systematic study, especially in experiment.

Thus, in this paper, we conduct a comprehensive investigation on trapping force and stability of circular swallowtail beams. Initially, we delve into the autofocusing characteristics of circular swallowtail beams through both experimental and theoretical approaches. Subsequently, we extend our analysis to the trapping performance on Rayleigh particles, providing theoretical insights into the trapping forces exerted by CSBs. To validate our findings, we employ CSBs as optical tweezers in experimental, trapping particles and measuring the optical trap stiffness. Remarkably, our measured values agree well with those calculated using Generalized Lorentzian Mie theory, confirming the accuracy and reliability of CSBs in optical trapping applications. This work significantly contributes to the understanding of the optical trapping capabilities of CSBs, paving the way for the application of these innovative tools in optical manipulation and trapping scenarios.

II. PROPAGATION OF CSBS

Based on catastrophe theory, a caustic field with standard diffraction integral is given by[14]:

$$\psi_n(\mathbf{a}) = \int_{-\infty}^{+\infty} \exp[ip_n(\mathbf{a}, s)] ds \quad (1)$$

where $p_n(\mathbf{a}, s)$ is the canonical potential function that can determine the properties of the caustic field, and it is defined by[14]:

$$p_n(\mathbf{a}, s) = s^n + \sum_{j=1}^{n-2} a_j s^j \quad (2)$$

Here, $\mathbf{a} = (a_1, a_2, \dots, a_j)$ is the control parameter and s is the state parameter. Usually, a Swallowtail beam can

* liangyi@gxu.edu.cn

be expressed by the swallowtail catastrophe integral[27]:

$$Sw(X, Y, Z) = \int_{-\infty}^{+\infty} \exp([i(s^5 + Zs^3 + Ys^2 + Xs^1)]) ds \quad (3)$$

where X, Y, Z denotes the dimensionless coordinates in the real space.

For simply constructing a circular swallowtail beam, Eq.3 is transformed into a expression in cylindrical coordinates[27]:

$$\Phi(r, \theta, 0) = Sw\left(\frac{r_0 - r}{w_0}, 0, 0\right) Q(r, \theta) \quad (4)$$

where r_0 is the initial radius of the main ring and w_0 is the scale factor, which determines the numbers and width of ring. $Q(r, \theta)$ is the optical aperture to make the energy of beam finite for experimental realization. It restricts the beams within given region and is defined as follows:

$$Q(r, \theta) = \begin{cases} 1, & 0 \leq r \leq R_B, 0 \leq \theta \leq 2\pi \\ 0, & \text{other.} \end{cases} \quad (5)$$

where R_B is the radius of the CSBs in the initial plane.

In paraxial approximation, Swallowtail beam propagates following the below wave equation[27]:

$$2i \frac{\partial \Phi}{\partial \xi} + \frac{\partial^2 \Phi}{\partial r^2} + r^{-1} \frac{\partial \Phi}{\partial r} + r^{-2} \frac{\partial \Phi}{\partial \theta} = 0 \quad (6)$$

Then, similar to the previous works[32, 33]. We can apply beam propagation methods to simulate the propagation of CSBs and analyze their autofocusing property. In experiment, CSBs are generated by means of hologram, as shown in the Fig.1(a). The hologram is loaded in a transmissive spatial light modulator(SLM) (1024×768, pixel pitch is 36 μm , fill factor is 58%). A linear polarized Gaussian beam is emitted from the semiconductor laser (532 nm), and then are expanded by the lens (L1 and L2). After passing through the SLM, such beam is transferred into a CSB with sufficient information by a 4f system (L3 and L4). The initial intensity distribution of the CSBs appears in the focal plane of L4 and the propagation of CSBs can be recorded by moving the CCD camera. In the simulation and experiment, the parameters are set as $R_B=1.4$ mm, $r_0=0.7$ mm, $w_0=8.33$ μm , the incident power of simulation is kept as 1 W.

Figure1(b, c) display the numerical and experimental propagation results of CSBs including the intensity of propagation of CSBs at $z=0$ mm, 61 mm (z is the propagation distance) and their propagation sideview. Clearly, at the beginning, the main ring of CSBs possesses the maximum intensity when CSBs are generated in Fig.1(b1). When the beam comes to the position of $z=61$ mm [Fig.1(b2)], all power automatically focuses at a very small spot whose radius is about 10.5 μm , obviously exhibiting a autofocusing property without any

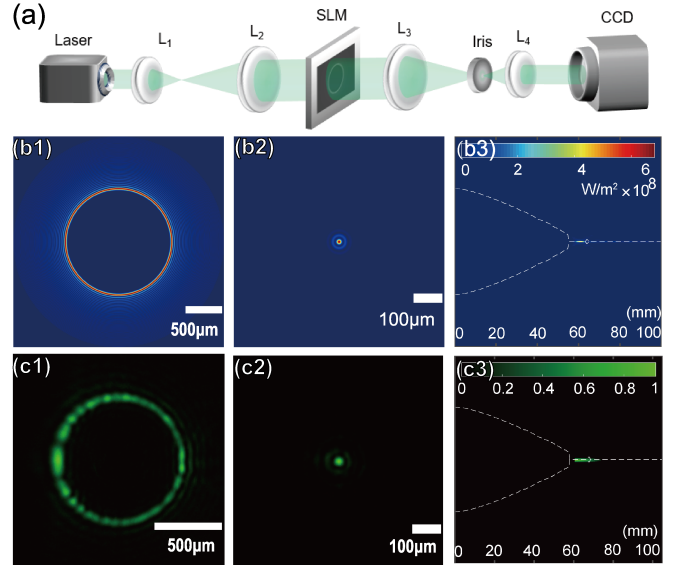


FIG. 1. Propagation of CSBs. (a) Experiment setup: Laser(532 nm), semiconductor laser. L, lens. SLM, spatial light modulator. (b1, b2) Numerical results at $z=0$ mm, 61 mm. (b3) Numerical propagation sideview. (c1-c3) corresponding experimental results.

lens in free space. Fig.1(b3,c3) are the sideview of propagation, the dash lines depict the trajectory of the main ring and autofocusing is observed clearly. One can find that the experiment are basically consistent with the simulation.

III. TRAPPING PERFORMANCE OF CSBS ON RAYLEIGH PARTICLE

According to the theory, the gradient force \vec{F}_g and the scattering force \vec{F}_s of Rayleigh particle can be calculated by[34]:

$$\vec{F}_g = \frac{1}{4} \epsilon_0 \epsilon_m \text{Re}(\alpha) \nabla |\vec{\Phi}^2| \quad (7)$$

$$\vec{F}_s = \frac{1}{6\pi c} \epsilon_m^3 k_0^4 |\alpha|^2 \vec{S} \quad (8)$$

where ϵ_m is the dielectric of the medium around the particle, ϵ_0 is the dielectric of the constant in vacuum, k_0 is the wave number, $\alpha = 4\pi R_P^3 (\epsilon_p - \epsilon_m) / (\epsilon_p + 2\epsilon_m)$ is polarizability (R_P is the radius of Rayleigh particles). \vec{S} is the Poynting vector, which can be calculated by[11, 35]:

$$\vec{S} = \vec{S}_z + \vec{S}_\perp = \frac{1}{2\eta_0} |\Phi^2| \hat{z} + \frac{i}{4\eta_0 k} [\Phi \nabla_\perp \Phi^* - \Phi^* \nabla_\perp \Phi] \quad (9)$$

where the $\eta_0 = \sqrt{\mu_0 / \epsilon_0}$ is the impedance of free space.

Figure 2 presents the calculated trapping force results of CSBs with a focal spot of 2.76 μm while they trap

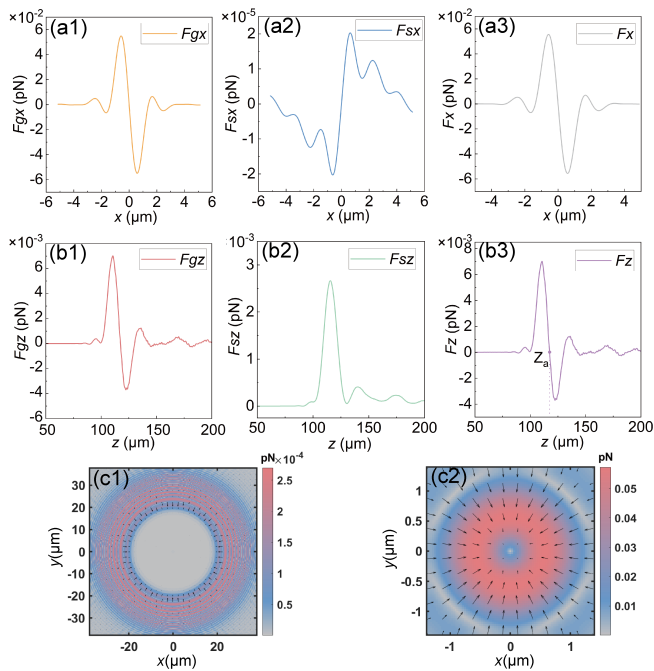


FIG. 2. Distribution of tapping force. The R_B is $50 \mu\text{m}$, the r_0 is $25 \mu\text{m}$, the w_0 is $0.7 \mu\text{m}$, the radius of polystyrene particles is 46 nm . The focal length is $116.29 \mu\text{m}$. $Z_a = 117.29 \mu\text{m}$ is the longitudinal trapping position. (a1) Transversal gradient force (F_{gx}) at Z_a . (a2) Transversal scattering force (F_{sx}) at Z_a . (a3) Transversal total force (F_x) at Z_a . (b1) Longitudinal gradient force (F_{gz}). (b2) Longitudinal scattering force (F_{sz}). (b3) Total Longitudinal force (F_z). (c1) Force distribution at $z=30 \mu\text{m}$. (c2) Force distribution at the focus.

Rayleigh polystyrene particles of $R_P = 46 \text{ nm}$ in water ($\varepsilon_m = 1.77$, $\varepsilon_p = 2.47$). As illustrated in Figs.2a(1, 2) and b(1, 2), both of transversal and longitudinal gradient forces are larger than the scattering force at the focus. Furthermore, we find that the maximum value of the total axial force exceeds than the difference between buoyancy and gravity (as calculated by us at $2 \times 10^{-10} \text{ pN}$, and 10^{-7} pN according to Ref.[25]). In this case, CSBs is possible to trap the above particles stably. Noted that, all force vectors are directed towards the center of the beams, indicating that there is only one transverse trapping position and all surrounding particles are pulled towards the center [Fig.2c(1,2)].

To further investigate the trapping stability of CSBs, we calculate the related parameters including the Brownian force F_b of trapped particle and the Boltzmann factor as follows[3, 25, 36]:

$$F_b = \sqrt{12\pi\eta R_p k_B T} \quad (10)$$

$$\xi = \exp(-U/k_B T) \quad (11)$$

where $U = \frac{1}{4}\varepsilon_0\varepsilon_m \text{Re}(\alpha)\Delta|\vec{\phi}^2|$ is the potential energy of gradient force, $\Delta|\vec{\phi}^2|$ denotes the intensity difference related to the potential energy of the gradient force, k_B

represents the Boltzmann constant, T is the thermodynamic temperature of medium (here, we assume that the $T = 300 \text{ K}$), η denotes the viscosity of the surrounding medium (Water, $\eta = 8 \times 10^{-4} \text{ Pa} \cdot \text{s}$).

TABLE I. Trapping stability analysis.

F_b (pN)	F_{gx} (pN)	F_{gz} (pN)	ξ
2.40×10^{-3}	5.32×10^{-2}	5.26×10^{-3}	1.94×10^{-5}

The calculation results related to the trapping stability are presented in Table.I. Clearly, both the transversal gradient force (F_{gx}) and longitudinal gradient forces (F_{gz}) can overcome the Brownian force (F_b). Moreover, the Boltzmann factor (ξ) is much less than 1, suggesting that the time to trap a particle is much less than the time to leave the trap due to Brownian motion[3]. Thus, it can be inferred that the above Rayleigh particles can be stably trapped by CSBs.

IV. TUNING THE AUTOFOCUSING AND TRAPPING FORCE PROPERTIES

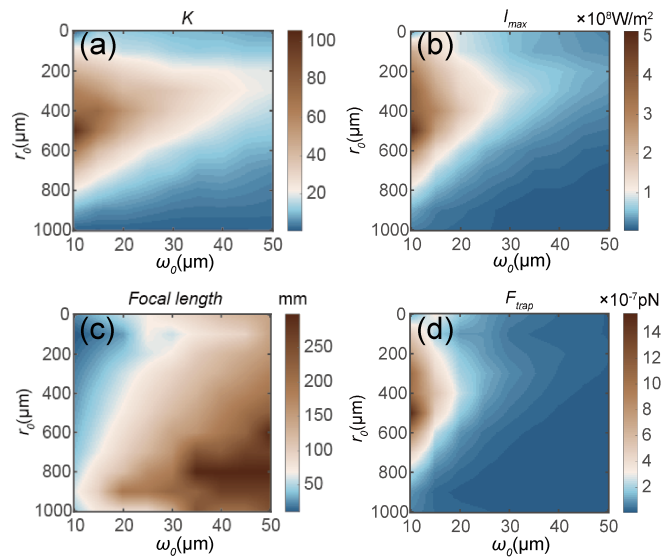


FIG. 3. Trapping-force performance of CSBs with varying parameters r_0 and w_0 . R_B is set to be 2 mm , the incident power is 1 W , the wavelength is 1064 nm , the radius of polystyrene particle is 20 nm . (a) The Autofocusing properties, $K = I_{max}/I_0$, I_{max} is the focal peak intensity, I_0 is the peak intensity of initial plane. (b) The focal peak intensity I_{max} . (c) The autofocusing length z . (d) The trapping-force F_{trap} .

As we know, the r_0 controls the radius of main ring in the source plane, and the w_0 controls the width of the main ring and the number of rings in the source plane. Both of them affect the focal spot size and further the

autofocusing intensity. Thus, by altering the parameters of CSBs in detail, we can analyze the quantitative changes in autofocusing and trapping force at the focus, as shown in Fig.3. From Fig.3, one can see that, the distribution of focal peak intensity (I_{max}) in Fig.3(b) is different from the intensity contrast K (K is the ratio between the maximum light intensity at the focal plane and the maximum light intensity at the initial plane) [Fig.3(a)]. However, both of focal peak intensity and intensity contrast can reach at a largest value when choosing appropriate r_0 while they decreases with increasing w_0 . During these changing, the autofocusing length keeps increasing and the trapping force following the variation of focal peak intensity [Fig.3(c, d)]. Especially, it is found that the theoretical optimal autofocusing and largest trapping force appears at $r_0 \approx 0.5R_B$ [Fig.3(d)]. Because the variation of the trapping force is larger than that of intensity contrast at the same conditions, trapping force is more sensitive to the influence of the parameters.

V. TRAPPING PERFORMANCE OF CSBS ON MIE PARTICLES

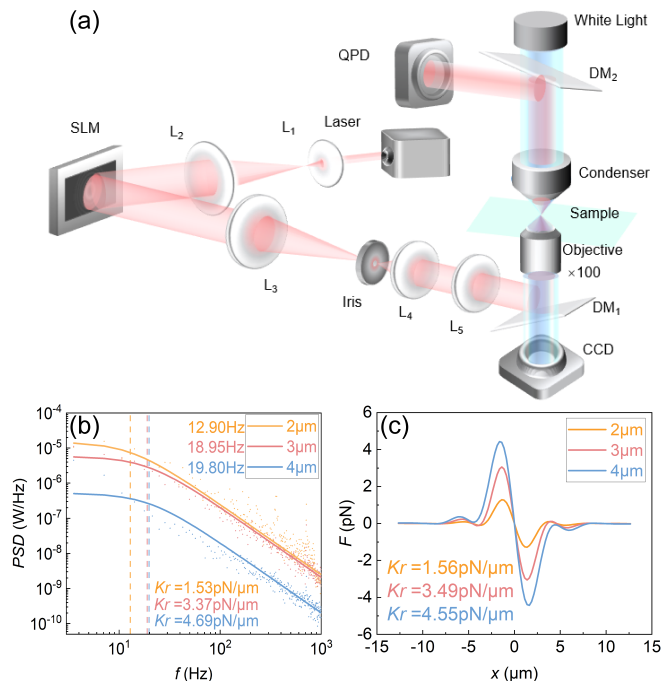


FIG. 4. The experiment setup for trapping and observing particles and the power spectra and trapping stiffness. Laser, wavelength is 1064 nm. SLM, Spatial Light Modulator. CCD, Charged Coupled Device. Objective, oil objective lens($\times 100$), the numerical aperture is 1.25. DM, Dichroic Mirror. QPD, quadrant photoelectric detector. Incident power is 20 mW. (b) Power spectra of trapping polystyrene particles with a diameter of 2-4 μm . (c) The trapping force distribution of Mie particles, and the trap stiffness is given.

Finally, to investigate the trapping performance of CSBs on Mie articles, we utilized the CSBs as optical tweezers to trap large polystyrene beads with different sizes in water (See video within the Supplemental Material [37]). As shown in [Fig.4(a)], we employed a similar experimental setup as in Refs. [33–35]: The CSB was generated at the focal plane of Lens 4 (source plane of the CSB), and subsequently relayed to the sample by using a 4-f imaging system comprised of Lens 5 and Oil Lens. After changing the distances between Len4 and Lens5, we placed the autofocusing position right at the focal point of Oil Lens. This allowed us to realize optical tweezers based on CSBs for trapping polystyrene beads. We then used power spectrum methods [33–35] to analyze the trap stiffnesses of the beams.

In detail, to measure the trap stiffness, we collected scattered light from beads using a condenser lens and a quadrant photodiode (QPD) to record the real-time positions of the trapped beads. These positions were then transformed into a power spectrum for calculating the trapping stiffness. Specifically, the trap stiffness ($\kappa_r = -dF_{trap}/dr$) of the beams was calculated from the experimental data of the real-time trapped bead positions using the Langevin equation and the corner frequency power spectrum ($f_{c,r}$): $f_{c,r} = \kappa_r/2\pi\gamma$. Here, γ represents the particle friction coefficient ($\gamma = 3\pi\eta D_P$), where η is the viscosity of the solution, and $D_P = 2R_P$ is the diameters of the trapped object.

Fig.4(b,c) present the experimental results of trap stiffness when the size of trapped particles changes from 2 μm to 4 μm (light power is 20 mW). The intersection of colored dash line and solid line [Fig.4(b)] represents the corner frequency. Clearly, trap stiffness increases with larger trapped Mie particles. In theory, since the size of experimental polystyrene bead is larger than wavelength, the full-wave generalized Lorenz-Mie theory and Maxwell stress tensor technique [33–35] are used to calculate the trapping force and stiffness.. As shown in Fig.4(c), the theoretical results are consistent with our experimental results. Trap stiffness still becomes larger when the size of trapped Mie particles increase.

VI. CONCLUSION

In summary, we conducted a systematic investigation into the tunable autofocusing propagation and trapping performance of CSBs by tuning the beam parameters. Our experimental results demonstrate that CSBs can trap well both Rayleigh particles and Mie particles. This work contributes to the development of optical trapping of autofocusing beams providing new photonic tools for optical tweezers and manipulation.

ACKNOWLEDGMENTS

This work was supported by the National Natural Science Foundation of China (11604058), the Guangxi Natural Science Foundation (2020GXNSFAA297041).

-
- [1] J. Chen, C. H. Wan, and Q. W. Zhan, Engineering photonic angular momentum with structured light: a review, *Advanced Photonics* **3** (2021).
- [2] Y. J. Yang, Y. X. Ren, M. Z. Chen, Y. Arita, and C. Rosales-Guzman, Optical trapping with structured light: a review, *Advanced Photonics* **3** (2021).
- [3] A. Ashkin, J. M. Dziedzic, J. E. Bjorkholm, and S. Chu, Observation of a single-beam gradient force optical trap for dielectric particles, *Optics letters* **11**, 288 (1986).
- [4] C. A. Campugan, K. R. Dunning, and K. Dholakia, Optical manipulation: a step change for biomedical science, *Contemporary Physics* **61**, 277 (2020).
- [5] Y. Liang, G. Liang, Y. X. Xiang, J. Lamstein, R. Gautam, A. Bezryadina, and Z. G. Chen, Manipulation and assessment of human red blood cells with tunable "tug-of-war" optical tweezers, *Physical Review Applied* **12** (2019).
- [6] P. Polimeno, A. Magazzu, M. A. Iati, R. Saija, L. Folco, D. B. Ciriza, M. G. Donato, A. Foti, P. G. Gucciardi, A. Saidi, C. Cecchi-Pestellini, A. J. Escobar, E. Ammannito, G. Sindoni, I. Bertini, V. D. Corte, L. Inno, A. Ciavarella, A. Rotundi, and O. M. Marago, Optical tweezers in a dusty universe, *European Physical Journal Plus* **136** (2021).
- [7] G. A. Siviloglou and D. N. Christodoulides, Accelerating finite energy airy beams, *Optics Letters* **32**, 979 (2007).
- [8] H. Cheng, W. P. Zang, W. Y. Zhou, and J. G. Tian, Analysis of optical trapping and propulsion of rayleigh particles using airy beam, *Optics Express* **18**, 20384 (2010).
- [9] Z. Zheng, B. F. Zhang, H. Chen, J. P. Ding, and H. T. Wang, Optical trapping with focused airy beams, *Applied Optics* **50**, 43 (2011).
- [10] I. Kaminer, M. Segev, and D. N. Christodoulides, Self-accelerating self-trapped optical beams, *Physical Review Letters* **106** (2011).
- [11] J. Broky, G. A. Siviloglou, A. Dogariu, and D. N. Christodoulides, Self-healing properties of optical airy beams, *Optics Express* **16**, 12880 (2008).
- [12] P. Zhang, J. Prakash, Z. Zhang, M. S. Mills, N. K. Efremidis, D. N. Christodoulides, and Z. G. Chen, Trapping and guiding microparticles with morphing autofocusing airy beams, *Optics Letters* **36**, 2883 (2011).
- [13] J. D. Ring, J. Lindberg, A. Mourka, M. Mazilu, K. Dholakia, and M. R. Dennis, Auto-focusing and self-healing of pearcey beams, *Optics Express* **20**, 18955 (2012).
- [14] A. Zannotti, F. Diebel, M. Boguslawski, and C. Denz, Optical catastrophes of the swallowtail and butterfly beams, *New Journal of Physics* **19** (2017).
- [15] Z. Sun, J. T. Hu, Y. S. Wang, W. N. Ye, Y. X. Qian, and X. Z. Li, Generation of high-dimensional caustic beams via phase holograms using angular spectral representation, *Optics Express* **31**, 7480 (2023).
- [16] N. C. Zhang, J. Q. Song, D. M. Li, X. Y. Tong, T. Li, M. L. Sun, X. X. Ma, X. Zhang, K. K. Huang, and X. H. Lu, Multi-focus autofocusing circular hyperbolic umbilic beams, *Optics Express* **30**, 32978 (2022).
- [17] Z. Sun, J. T. Hu, Y. S. Wang, W. N. Ye, and Y. X. Qian, Manipulating self-focusing beams induced by high-dimensional parabolic umbilic beams, *Results in Physics* **52**, 10.1016/j.rinp.2023.106806 (2023).
- [18] X. Y. Chen, D. M. Deng, J. L. Zhuang, X. Peng, D. D. Li, L. P. Zhang, F. Zhao, X. B. Yang, H. Z. Liu, and G. H. Wang, Focusing properties of circle pearcey beams, *Optics Letters* **43**, 3626 (2018).
- [19] A. Zannotti, F. Diebel, and C. Denz, Dynamics of the optical swallowtail catastrophe, *Optica* **4**, 1157 (2017).
- [20] M. A. Bandres and J. C. Gutierrez-Vega, Airy-gauss beams and their transformation by paraxial optical systems, *Optics Express* **15**, 16719 (2007).
- [21] G. A. Siviloglou, J. Broky, A. Dogariu, and D. N. Christodoulides, Observation of accelerating airy beams, *Physical Review Letters* **99** (2007).
- [22] H. I. Sztul and R. R. Alfano, The poynting vector and angular momentum of airy beams, *Optics Express* **16**, 9411 (2008).
- [23] E. Granot and B. Malomed, Acceleration of trapped particles and beams, *Journal of Physics B-Atomic Molecular and Optical Physics* **44** (2011).
- [24] N. K. Efremidis, Z. G. Chen, M. Segev, and D. N. Christodoulides, Airy beams and accelerating waves: an overview of recent advances, *Optica* **6**, 686 (2019).
- [25] Y. F. Jiang, K. K. Huang, and X. H. Lu, Radiation force of abruptly autofocusing airy beams on a rayleigh particle, *Optics Express* **21**, 24413 (2013).
- [26] K. Cheng, G. Lu, and X. Q. Zhong, The poynting vector and angular momentum density of swallowtail-gauss beams, *Optics Communications* **396**, 58 (2017).
- [27] H. A. Teng, Y. X. Qian, Y. P. Lan, and Y. M. Cai, Abruptly autofocusing circular swallowtail beams, *Optics Letters* **46**, 270 (2021).
- [28] H. A. Teng, Y. X. Qian, Y. P. Lan, and W. T. Cui, Swallowtail-type diffraction catastrophe beams, *Optics Express* **29**, 3786 (2021).
- [29] J. J. Jiang, D. L. Xu, Z. W. Mo, X. Z. Cai, H. Y. Huang, Y. Zhang, H. B. Yang, H. Q. Huang, Y. Wu, L. L. Shui, and D. M. Deng, Generation and control of tornado waves by means of ring swallowtail vortex beams, *Optics Express* **30**, 11331 (2022).
- [30] Y. Wu, Z. J. Lin, C. J. Xu, D. L. Xu, H. Q. Huang, J. J. Zhao, Z. W. Mo, J. J. Jiang, H. B. Yang, L. P. Zhang, H. Z. Liu, D. M. Deng, and L. L. Shui, Abruptly autofocusing twisted optical bottle beams, *Physical Review Applied* **17** (2022).
- [31] Y. Zhang, J. L. Tu, S. L. He, Y. P. Ding, Z. L. Lu, Y. Wu, G. H. Wang, X. B. Yang, and D. M. Deng, Experimental generation of the polycyclic tornado circular swallowtail beam with self-healing and auto-focusing, *Optics Express* **30**, 1829 (2022).

- [32] F. Lu, L. Tan, Z. Tan, H. Wu, and Y. Liang, Dynamical power flow and trapping-force properties of two-dimensional airy-beam superpositions, *Physical Review A* **104** (2021).
- [33] F. Lu, H. Wu, Y. Liang, L. Tan, Z. Tan, X. Feng, Y. Hu, Y. Xiang, X. Hu, Z. Chen, and J. Xu, Bessel-modulated autofocusing beams for optimal trapping implementation, *Physical Review A* **104** (2021).
- [34] Y. Liang, L. Tan, N. A. Liu, K. J. Chen, H. P. Liang, H. H. Wu, B. S. Luo, F. X. Lu, H. H. Chen, B. S. Zou, and P. L. Hong, Tunable autofocusing and enhanced trapping forces with circular pearcey airy beams, *Physical Review Applied* **19** (2023).
- [35] L. Tan, N. A. Liu, F. X. Lu, D. M. Liu, B. B. Yu, Y. T. Li, H. Wu, K. J. Chen, Y. Z. Chu, P. L. Hong, and Y. Liang, Quantitative characterization of autofocusing and trapping of multi-airy vortex beams, *Physical Review A* **107** (2023).
- [36] Z. Liu, X. Wang, and K. Hang, Enhancement of trapping efficiency by utilizing a hollow sinh-gaussian beam, *Scientific Reports* **9** (2019).
- [37] See supplemental material at [url will be inserted by publisher] for the video of trapping particles and moving them around.